 CMES, vol.24, no.3, pp.215-238, 2008

DFT Studies on Ferroelectric Ceramics and Their Alloys: $BaTiO_3$, $PbTiO_3$, $SrTiO_3$, $AgNbO_3$, $AgTaO_3$, $Pb_xBa_{1-x}TiO_3$ and $Sr_xBa_{1-x}TiO_3$

Mustafa Uludoğan[1], D. Paula Guarin[1], Zully E. Gomez[1], Tahir Cagin[1] and William A. Goddard III[2]

Abstract: Aiming at a presentation of the utility of the state of art of first-principles methods (PBE flavor of Density Functional Theory, DFT) in the area of materials science and engineering, we present our studies of the equation of state and ferroelectric-paraelectricphase transition in several ferroelectric systems, including $BaTiO_3$, $PbTiO_3$, $SrTiO_3$, $AgNbO_3$, $Pb_xBa_{1-x}TiO_3$ and $Sr_xBa_{1-x}TiO_3$. We also report the Born effective charges, optical dielectric constant, and phonon dispersion relation properties from Density Functional Perturbation Theory. Computed results are compared with other theoretical results (which were mostly on $BaTiO_3$, $PbTiO_3$, cubic $SrTiO_3$) using various approaches, as well as experiments. The studies on $AgNbO_3$and alloys are the first calculations to the best of our knowledge. The predictions obtained by DFT studies presented are in good agreement with the experimental results.

1 Introduction

Since the discovery of ferroelectricity in Rochelle salt crystal (Valasek, 1921) by Valasek in 1921, followed by the discovery of the ferroelectricity in ABO_3 perovskite $BaTiO_3$ (Gray, 1949) in 1945, new materials have successfully been designed for a variety of industrial and commercial applications such as high-dielectric constant capacitors, ferroelectric thin film memories, piezoelectric sonars, positive temperature coefficient sensors and switches. Thus, understanding the basics of ferroelectricity from quantum mechanical (QM) approaches and the use of this quantum mechanical data for the generation of a polarizable force fileds (FF) becomes a critical issue. $BaTiO_3$, $PbTiO_3$, $SrTiO_3$, $AgNbO_3$, $AgTaO_3$, $Pb_xBa_{1-x}TiO_3$ and $Sr_xBa_{1-x}TiO_3$ are the systems of interest to be characterized by QM calculations in terms of fundamental interactions and energetics. Calculations using DFT have been performed to understand the experimentally available phase transitions. For example, $BaTiO_3$ exhibits three ferroelectric phase transitions from cubic to tetragonal, from tetragonal to orthorhombic and finally from orthorhombic to rhombohedral as the temperature decreases.

The foremost aim of this work is to create systematic and reliable data to provide the basis for develoing force fields (FF) suitable for modeling domain boundaries and dynamic response of ferroelectric materials.

In the following section, details of the calculations will be presented. Methods used, details of the structures and optimization procedure for internal degrees of freedom for each structure will be discussed in this section. In Sec.III.A, results of the structure optimization, EOS, will be presented. Correspondence between this work and the experiment and other theoretical works will be shown. In Sec.III.B, importance of Born effective charges on bonding, ferroelectricity and Longitudinal optical- Transverse Optical (LO-TO) mode splitting will be addressed.

2 Methods of Calculation

Calculations of equations of state (EOS) have been performed in the general framework of DFT (Hohenberg & Kohn, 1964; Kohn & Sham, 1965; Payne, Teter, Allan, Arias, & Joannopoulos, 1992) using projector augmented wave method (PAW) (Kresse & Joubert, 1999). Exchange-correlation used was Perdew-Burke-Ernzerhof

[1] Texas A&M University, Artie McFerrin Department of Chemical Engineering, 519 Jack E. Brown Engineering Building, 3122 TAMU, College Station, TX 77843-3122

[2] Materials and Process Simulation Center, California Institute of Technology, Pasadena CA 91125

(PBE) (Perdew, Burke, & Ernzerhof, 1996) generalized gradient approximation (GGA). Kinetic energy cutoff of the electronic wavefunctions was expanded in plane waves up to 600 eV. Integrals over the Brillouin zone were summed on a Monkhorst-Pack mesh (Monkhorst & Paack, 1977) of $10\times10\times10$. The 5s, 5p and 6s levels of Ba, the 3s, 3p, 3d and 4s of Ti, the 2s and 2p of O, 4d and 5s of Ag, 4s, 4p, 4d and 5s of Nb, 4s, 4p and 5s of Sr, 5d, 6s and 6p of Pb were treated as valence states. Vienna Ab-initio software package, VASP (Kresse & Furthmüller, 1996; Kresse & Hafner, 1993) was used for the EOS and structural optimization calculations.

Most of ABO_3 type perovskites have similar stable phases at various temperatures. $BaTiO_3$ has four stable phases, namely, rhombohedral, orthorhombic, tetragonal and cubic phases at temperatures in the increasing order while $PbTiO_3$ has only two stable phases of tetragonal and cubic. All of these phases have some internal degrees of freedom (except cubic phase) that need to be optimized. Thus, DFT calculations have been performed at high precision (high kinetic energy cutoff and Monkhorst-Pack mesh) in order to obtain the ferroelectric phases precisely. No minimization was done in cubic phase. At desired volume, total energy and diagonal hydrostatic pressure tensor were obtained. Volume of the cubic cell was expanded 10 % and was contracted 15 % with respect to zero pressure state in order to get the EOS. EOS used in the calculations was Rose's universal binding curve (Rose, Smith, Guinea, & Ferrante, 1984). In the ferroelectric phases, the optimization procedure of the structures was rather complicated since number of degrees of freedom increased for the lower symmetry structures. Tetragonal, orthorhombic and rhombohedral structures contained respectively four, six and 5 atomic degrees of freedom. A conjugate-gradient algorithm (Press, Flannery, Teukolsky, & Vetterling, 1986) was used for minimization process. First of all, ions were relaxed into their instantaneous ground state by keeping the volume and cell shape fixed. Then with the relaxed positions, only the cell shape was optimized at fixed volume. This minimization process has been followed at constant volume since the forces between ions were less than 0.001 eV/A. The same procedure is followed for the volumes up to 10 % expansion and down to 15 % contraction of the zero pressure state.

For cubic structure, there was no need for minimization. Tetragonal structure was optimized by letting the fractional coordinates of the ions change in the way symmetry allows (distortion in z direction) at fixed c/a ratio by keeping the volume fixed. Then, by using the optimized fractional coordinates of the ions, c/a ratio was optimized at constant volume. Thus, c/a ratio,$\Delta_{T,Z}$[Ti], $\Delta_{T,Z}$[O(1)] and $\Delta_{T,Z}$[O(2)] were the quantities that were optimized during the minimization. In orthorhombic phase, lattice parameters a, b, c and$\Delta_{O,Z}$[Ti], $\Delta_{O,Z}$[O(1)], $\Delta_{O,Y}$[O(2)] and $\Delta_{O,Z}$[O(2)] were the degrees of freedom. Lattice parameter a (a=b=c), the angle α ($\alpha=\beta=\gamma$), $\Delta_{R,Z}$[Ti], $\Delta_{R,Z}$[O], and $\Delta_{R,X}$[O] were the optimized quantities for rhombohedral phase. Similar optimization scheme with tetragonal phase was used in orthorhombic and rhombohedral phases. Atomic positions are shown in Table 1.

$SrTiO_3$ has point group symmetry of *I4/mcm* in tetragonal structure which is different than the point group symmetry *P4mm* of tetragonal $BaTiO_3$ and $PbTiO_3$. Calculations have been performed with a molecular unit of four which has two degrees of freedom to be optimized, namely c/a ratio and x, distortion in fractional coordinates. Atomic positions are shown in Table 2.

$AgNbO_3$ has point group symmetry of *P4/mbm* in tetragonal structure. Calculations have been performed with the unit cell which has two degrees of freedom to be optimized, namely c/a ratio and x, distortion in fractional coordinates. Atomic positions are shown in Table 3.

ABINIT ab initio software package (Gonze et al., 2002; Gonze et al., 2005) was employed in order to obtain response function calculations within the recent advances in density functional theory. Within ABINIT, PBE exchange-correlation formalism with a norm-conserving pseudo-potential approach (Grinberg, Ramer, & Rappe, 2000; Rappe, Rabe, Kaxiras, & Joannopoulos, 1990) was used with the same valence states defined

Table 1: The atomic positions of ABO_3 (A=Ba, Pb, B=Ti) type perovskite for the cubic, tetragonal, orthorhombic and rhombohedral structures in fractional coordinates. The "A" atom is located at the (0,0,0) position. $\Delta_{T,Z}[Ti]$, $\Delta_{T,Z}[O(1)]$, and $\Delta_{T,Z}[O(2)]$ represent the distortions of Ti and O atoms in the tetragonal structure, respectively (Hellwege & Hellwege, 1969). Similarly, in the orthorhombic structure, $\Delta_{O,Z}[Ti]$, $\Delta_{O,Z}[O(1)]$, $\Delta_{O,Z}[O(2)]$ and $\Delta_{O,Y}[O(2)]$ are the distortions for Ti and O atoms (Hellwege & Hellwege, 1969). Finally, in rhombohedral structure, $\Delta_{R,Z}[Ti]$, $\Delta_{R,Z}[O]$, and $\Delta_{R,X}[O]$ are the distortions for Ti and O atoms (Ghosez, Gonze, & Michenaud, 1999).

Cubic	Atom	Position
	Ba	(0.0,0.0,0.0)
	Ti	(0.5,0.5,0.5)
	O_1	(0.5,0.5,0.0)
	O_2	(0.5,0.0,0.5)
	O_3	(0.0,0.5,0.5)
Tetragonal	Ba	(0.0,0.0,0.0)
	Ti	(0.5,0.5,0.5+$\Delta_{T,Z}$[Ti]
	O_1	(0.5,0.0,0.5+$\Delta_{T,Z}$[O(1)])
	O_2	(0.5,0.0,0.5+$\Delta_{T,Z}$[O(2)])
	O_3	(0.0,0.5,0.5+$\Delta_{T,Z}$[O(2)])
Orthorhombic	Ba	(0.0,0.0,0.0)
	Ba	(0.0,0.5,0.5)
	Ti	(0.5,0.0,0.5+$\Delta_{O,Z}$[Ti])
	Ti	(0.5,0.5,0.0+$\Delta_{O,Z}$[Ti])
	O(1)	(0.0,0.0,0.5+$\Delta_{O,Z}$[O(1)])
	O(1)	(0.0,0.5,0.0+$\Delta_{O,Z}$[O(1)])
	O(2)	(0.5,0.25+$\Delta_{O,Y}$[O(2)],0.25+$\Delta_{O,Z}$[O(2)])
	O(2)	(0.5,0.75+$\Delta_{O,Y}$[O(2)],0.75+$\Delta_{O,Z}$[O(2)])
	O(2)	(0.5,0.75-$\Delta_{O,Y}$[O(2)],0.25+$\Delta_{O,Z}$[O(2)])
	O(2)	(0.5,0.25-$\Delta_{O,Y}$[O(2)],0.75+$\Delta_{O,Z}$[O(2)])
Rhombohedral	Ba	(0.0,0.0,0.0)
	Ti	(0.5+$\Delta_{R,Z}$[Ti],0.5+$\Delta_{R,Z}$[Ti],0.5+$\Delta_{R,Z}$[Ti])
	O_1	(0.5+$\Delta_{R,Z}$[O],0.5+$\Delta_{R,Z}$[O],0.0+$\Delta_{R,X}$[O])
	O_2	(0.5+$\Delta_{R,Z}$[O],0.0+$\Delta_{R,X}$[O],0.5+$\Delta_{R,Z}$[O])
	O_3	(0.0+$\Delta_{R,X}$[O],0.5+$\Delta_{R,Z}$[O],0.5+$\Delta_{R,Z}$[O])

above. Electronic wave functions were expanded in plane waves up to 1360 eV. 4x4x4 Monkhorst-Pack mesh was accurate enough to sample the Brillouin Zone.

Dynamical matrix, Born effective charges and dielectric tensor were computed within a variational formulation (Gonze, Allan, & Teter, 1992; Lee, Ghosez, & Gonze, 1994) of the density functional perturbation theory (Baroni, Giannozzi, & Testa, 1987; Zein, 1984). First, calculations were carried out to determine the dynamical matrix on different meshes of q-points. Then, an interpolation was performed following the scheme proposed in (Giannozzi, de Gironcoli, Pavone, & Baroni, 1991; Gonze, Charlier, Allan, & Teter, 1994). In this approach, the long-range character of the dipole-dipole contribution was subtracted from the force constant matrix in reciprocal space.

Table 2: The atomic positions for $SrTiO_3$ in tetragonal phase of I4/mcm point group symmetry (Henry & Lonsdale, 1952). Ti atom is located at (0,0,0) position. Tetragonal cell contains four (Z=4) molecular units. x_T represents the distortion of Oxygen atoms.

Atom	Position
Sr(1)	(0, ½, ¼)
Sr(2)	(½, 0, ¾)
Sr(3)	(½, 0, ¼)
Sr(4)	(0, ½, ¾)
Ti(1)	(0, 0, 0)
Ti(2)	(½,½, 0)
Ti(3)	(0, 0, ½)
Ti(4)	(½, ½, ½)
$O_1(1)$	(0, 0, ¼)
$O_1(2)$	(½, ½,¾)
$O_1(3)$	(0, 0, ¾)
$O_1(4)$	(½, ½,¼)
$O_2(1)$	(x_T , ½+ x_T , 0)
$O_2(2)$	($\overline{x}_T$,½- x_T , 0)
$O_2(3)$	(½+ x_T , $\overline{x}_T$, 0)
$O_2(4)$	(½- x_T , x_T , 0)
$O_2(5)$	(½+ x_T , x_T , ½)
$O_2(6)$	(½- x_T , $\overline{x}_T$, ½)
$O_2(7)$	(x_T , ½- x_T , ½)
$O_2(8)$	($\overline{x}_T$,½+ x_T , ½)

Then the short range contribution to the interatomic force constants in real space is obtained from the remainder of the force constant matrix in q space using a discrete Fourier transformation (Ghosez, Cockayne, Waghmare, & Rabe, 1999; Ghosez, Gonze, & Michenaud, 1998).

3 Results

3.1 Equations of State

As being the first ferroelectric ceramic discovered in early 1940s, $BaTiO_3$ has been one of the most studied cubic perovskites since then. It is paraelectric at high temperature and it has the simple cubic perovskite structure. Its structure becomes

Table 3: Wyckoff notations of atomic positions for $AgNbO_3$ in tetragonal phase of P4/mbm point group symmetry (Henry & Lonsdale, 1952). Nb atom is located at (0,0,0) position. Tetragonal cell contains two (Z=2) molecular units where x_T represents the distortion for O atoms.

Atom	Position
Ag(1)	(0, ½, ½)
Ag(2)	(½, 0, ½)
Nb(1)	(0, 0, 0)
Nb(2)	(½, ½ ,0)
$O_1(1)$	(0, 0, ½)
$O_1(2)$	(½, ½, ½)
$O_2(1)$	(x_T , ½+ x_T , 0)
$O_2(2)$	($\overline{x}_T$, ½- x_T , 0)
$O_2(3)$	(½+ x_T , $\overline{x}_T$, 0)
$O_2(4)$	(½- x_T , x_T , 0)

tetragonal, orthorhombic and rhombohedral as the temperature of the system decreases. At T=130 °C, the cubic structure (m3m point group) transforms into a tetragonal structure (4mm). At 5°C, the tetragonal structure transforms into a structure with orthorhombic symmetry (mm2). Finally, the phase transition from orthorhombic to rhombohedral phase (3m) takes place at -90°C. Each transition is accompanied with small atomic displacements, latent heats and macroscopic strains along the ferroelectric direction. In the ferroelectric phases, the polar axis is aligned from tetragonal phase to rhombohedral phase along the $< 100 >$, $< 110 >$, and $< 111 >$ directions respectively.

There have been numerous efforts to calculate the bulk properties of barium-titanate from ab-initio calculations. In addition to developing a comprehensive description of phases and propertieies of $BaTiO_3$ we also aimed to obtain accurate data from DFT for generating Polarizable Charge Equilibration (P-QEq) force field (Zhang, 2004) parameters. This force field includes self-consistent atomic polarization and charge transfer in molecular dynamics of materials. Details of this force field and the optimization procedure are

Table 4: Wyckoff notations of atomic positions for $AgNbO_3$ in orthorhombic phase of Cmcm point group symmetry (Henry & Lonsdale, 1952). Orhorhombic cell contains eight (Z=8) molecular units. $y_{O_1,Ag(1)}$ and $y_{O_1,Ag(2)}$ are the corresponding distortions for Ag(1) and Ag(2) atoms in y-direction in orthorhombic phase, respectively. Other distortions can be defined with this manner.

Atom	Position
Ag(1)	$(0,\ y_{O_1,Ag(1)},\ ¼)$
	$(0, \overline{y}_{O_1,Ag(1)},\ ¾)$
	$(½,\ y_{O_1,Ag(1)} + ½,\ ¼)$
	$(½,\ ½\text{-}\ y_{O_1,Ag(1)},¾)$
Ag(2)	$(0,\ y_{O_1,Ag(2)},\ ¼)$
	$(0, \overline{y}_{O_1,Ag(2)},\ ¾)$
	$(½,\ y_{O_1,Ag(2)} + ½,\ ¼)$
	$(½,\ ½\text{-}\ y_{O_1,Ag(2)},¾)$
Nb	(¼, ¼, 0) (¼, ¾, 0) (¼,¼, ½) (¼, ¾, ½) (¾, ¾, 0) (¾, ¼, 0) (¾, ¾, ½) (¾, ¼, ½)
O(1)	$(x_{O_1,O(1)}, 0, 0)$
	$(\overline{x}_{O_1,O(1)}, 0, 0)$
	$(x_{O_1,O(1)}, 0, ½)$
	$(\overline{x}_{O_1,O(1)}, 0, ½)$
	$(x_{O_1,O(1)} + ½, ½, 0)$
	$(\overline{x}_{O_1,O(1)} + ½, ½, 0)$
	$(x_{O_1,O(1)} + ½, ½, ½)$
	$(\overline{x}_{O_1,O(1)} +½, ½, ½)$
O(2)	$(0,\ y_{O_1,O(2)},\ z_{O_1,O(2)})$
	$(0,\ \overline{y}_{O_1,O(2)},\ \overline{z}_{O_1,O(2)})$
	$(0,\ y_{O_1,O(2)},\ ½\text{-}z_{O_1,O(2)})$
	$(0,\ \overline{y}_{O_1,O(2)},\ ½+z_{O_1,O(2)})$
	$(½, y_{O_1,O(2)}+½,\ z_{O_1,O(2)})$
	$(½, \overline{y}_{O_1,O(2)}+½,\ \overline{z}_{O_1,O(2)})$
	$(½, y_{O_1,O(2)}+½,\ ½\text{-}z_{O_1,O(2)})$
	$(½, \overline{y}_{O_1,O(2)}+½,\ ½+z_{O_1,O(2)})$
O(3)	$(x_{O_1,O(3)},\ y_{O_1,O(3)},\ ¼)$
	$(\overline{x}_{O_1,O(3)}, y_{O_1,O(3)},\ ¼)$
	$(x_{O_1,O(3)}, \overline{y}_{O_1,O(3)},\ ¾)$

given elsewhere.

Energy-volume behaviors of the different crystalline phases of $BaTiO_3$ are shown in Figure 1. The data on energetics of the system supports that lowest symmetry structure is the structure with the lowest energy. The equations of state (EOS) results are tabulated in Table 4. The structural parameters are given in the Tables 5 through 7. Equilibrium volume and bulk modulus of the cubic structure obtained in this work is in good agreement with experiment. As expected, the local density approximation (LDA) results underestimate the equilibrium volume. The calculated cohesive energy in this work as well as the other theoretical calculations are systematically higher than the experiments (Uludoğan, Cagin, & Goddard III, 2002). To improve the value of calculated cohesive energy the authors in reference 29, performed calculation of cohesive energy by expanding the volume of the system of interest to seven times to that of the equilibrium volume. Still the DFT calculations overestimate the binding energy.

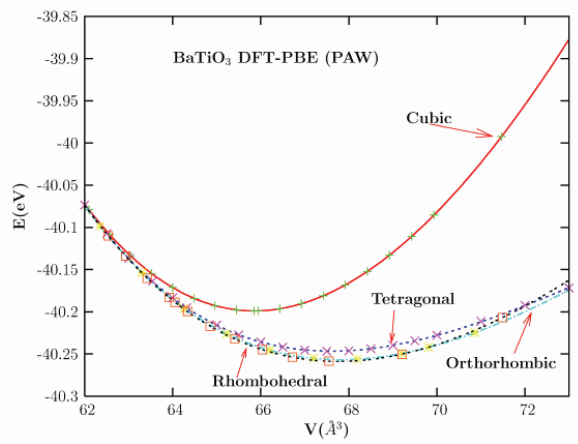

Figure 1: Energy as a function of volume for the cubic, tetragonal, orthorhombic and rhombohedral phases of $BaTiO_3$ from ab-initio calculations using DFT-PBE. Curves stand for the EOS fitting.

In Tables 5-7, the cell parameters and optimized fractional atomic coordinates for tetragonal, orthorhombic and rhombohedral structures of $BaTiO_3$ were given. Most of the earlier theoretical work (Frazer, 1962; Ghosez, Gonze et al.,

Table 5: EOS parameters of $BaTiO_3$ for the cubic, tetragonal, orthorhombic and rhombohedral structures: volume (lattice constant), cohesive energy, B, bulk modulus and B', pressure derivative of bulk modulus.

	$V_0(A^3)$	E_{COH}(eV)	B(GPa)	B'	Reference
Cubic	64.00	31.57	162		Exp.(Hellwege & Hellwege, 1969)
			135	6.4	Exp.(Pruzan et al., 2002)
	65.85	40.20	160.84	4.50	Present Work
	64.28	37.92	167.64	4.45	DFT-PW91(Uludoğan et al., 2002)
	61.30	38.23	189.00		DFT-LDA(Ghosez, Gonze et al.,
	60.93		194.2	3.68	1999)
	65.45		169		DFT-LDA(Khenata et al., 2005)
	65.45		175		DFT-GGA(Piskunov, Heifets, Eglitis, & Borstel, 2004)
					DFT-PBE(Piskunov et al., 2004)
Tetragonal	67.50	40.25	82.94		Present Work
	65.95	37.96	98.60		DFT-PW91(Uludoğan et al., 2002)
Orthorhombic	67.81	40.26	87.39		Present Work
	66.02	37.97	97.54		DFT-PW91(Uludoğan et al., 2002)
Rhombohedral	67.76	40.26	94.62		Present Work
	65.99	37.97	103.50		DFT-PW91(Uludoğan et al., 2002)

Table 6: Lattice parameters and atomic displacements in the tetragonal phase of $BaTiO_3$.

A(A)	c(A)	$\Delta_{T,Z}$[Ti]	$\Delta_{T,Z}$[O(1)]	$\Delta_{T,Z}$[O(2)]	Reference
3.99095	4.0352	0.0224	-0.0244	-0.0105	Exp. At 27 ° C (Kwei, Lawson,
4.00480	4.2087	0.0177	-0.0402	-0.0234	Billinge, & Cheong, 1993).
3.9759	4.1722	0.0188	-0.0473	-0.0266	Present Work (P=0 GPa)
3.99095	4.0352	0.0142	-0.0227	-0.0142	GGA-PW91 (P=0
3.99095	4.0352	0.0165	-0.0272	-0.0156	GPa)(Uludoğan et al., 2002)
3.994	4.036	0.0143	-0.0307	-0.0186	Present Work (Exp. Volume)
3.986	4.026	0.015	-0.023	-0.014	GGA-PW91 (Exp.
		0.014	-0.0249	-0.0156	volume)(Uludoğan et al., 2002)
		0.0135	-0.0250	-0.0150	LDA (Exp. volume)(Ghosez,
4.000	4.000	0.0138	-0.0253	-0.0143	Gonze et al., 1999)
					Exp.(Shirane, Danner, & Pepinsky, 1957)
					(Frazer, 1962)
					(Harada, Pedersen, & Barnea, 1970)
					(King-Smith & Vanderbilt, 1992)

1999; Harada et al., 1970; King-Smith & Vanderbilt, 1992) were performed with LDA exchange-correlation formalism. Within the LDA framework, the equilibrium volumes of ferroelectric phases were generally underestimated. Ferroelectric instability almost vanished at optimized structures of LDA because of being sensitive to the volume changes (Ghosez, Gonze et al., 1999). This is one of the reason why LDA calculations were performed at the experimental lattice constants. On the other hand the GGA calculations overestimate the equilibrium volume of paraelectric and ferroelectric phases. In tetragonal phase of $BaTiO_3$, the present work overestimated the c/a ratio as 1.051 while the experimental value was 1.011. Atomic distortions of LDA and GGA at

Table 7: Lattice parameters and atomic displacements of $BaTiO_3$ in orthorhombic phase.

	Exp.(Kwei et al., 1993) -43 °C	LDA(Ghosez, Gonze et al., 1999)	Exp.(Shirane et al., 1957) -10 °C	Present Work	Present Work Exp.Vol.
a(A)	3.9841	3.984	3.990	3.9914	3.9841
b(A)	5.6741	5.674	5.669	5.7830	5.6741
c(A)	5.6916	5.692	5.682	5.8223	5.6916
$\Delta_{O,Z}$[Ti]	0.0079	0.0127	0.010	0.0159	0.0121
$\Delta_{O,Z}$[O(1)]	-0.0233	-0.0230	-0.016	-0.0206	-0.0125
$\Delta_{O,Z}$[O(2)]	-0.0146	-0.0162	-0.010	0.0234	0.0149
$\Delta_{O,Z}$[O(3)]	-0.0145	-0.0146	-0.010	-0.0075	-0.0037

Table 8: Lattice parameters and atomic displacements of $BaTiO_3$ in rhombohedral phase.

a(A)	α (deg)	$\Delta_{R,Z}$[Ti]	$\Delta_{R,X}$[O]	$\Delta_{R,Z}$[O]	Reference
4.003	89.84	-0.013	0.011	0.0191	Exp.(Kwei et al., 1993)
4.001	89.87	-0.011	0.013	0.0192	(Ghosez, Gonze et al., 1999)
4.000	90.00	-0.012	0.010	0.0195	(King-Smith & Vanderbilt, 1992)
4.073	89.74	-0.0150	0.0141	0.0245	Present Work
4.042	89.77	-0.0148	0.0137	0.0246	(Uludoğan et al., 2002)

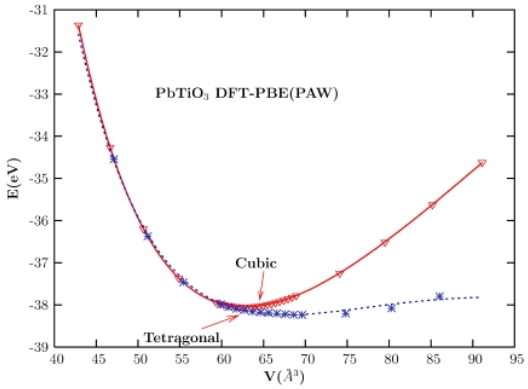

Figure 2: Energy as a function of volume for the cubic and tetragonal phases of $PbTiO_3$ from ab-initio calculations using DFT-PBE. Curves stand for the EOS fitting.

experimental lattice constants compared well with experiment.

At low temperatures, $PbTiO_3$ has a tetragonal perovskite structure. Tetragonal (P4mm) to cubic (Pm3m) phase transition occurs at 490 °C. Although $PbTiO_3$ has the same group symmetries with $BaTiO_3$ in tetragonal and cubic phases, they differ in terms of ferroelectric natures. $PbTiO_3$ has only one ferroelectric phase in the $< 100 >$ direction. Energy-volume behavior of tetragonal and cubic phases is shown in Figure 2. Tetragonal phase has the lowest energy structure satisfying the experiment.

In Table 8, the fractional atomic coordinates obtained from the experiment and theory were tabulated for tetragonal $PbTiO_3$. Despite the zero stress results of this work being far from experiment in terms of c/a ratio, atomic distortions calculated at the experimental volume with fixed lattice constants compare well with experiment.

$SrTiO_3$ has the same point group symmetry with $BaTiO_3$ and $PbTiO_3$ in cubic structure at high temperature. Cubic to tetragonal phase transition occurs at -168 °C. This low temperature phase transition is accompanied with antiferrodistortive transition. In Figure 3, energy volume behavior of cubic and tetragonal phases of $SrTiO_3$ is plotted.

For $AgNbO_3$, the stable phases from experiment is somehow cumbersome (Sciau, Kania, Dkhil,

Table 9: Lattice parameters and atomic displacements in the tetragonal phase of $PbTiO_3$.

A(A)	c(A)	$\Delta_{T,Z}$[Ti]	$\Delta_{T,Z}$[O(1)]	$\Delta_{T,Z}$[O(2)]	Reference
3.9016	4.1552	0.040	0.112	0.112	Exp.(Hellwege & Hellwege, 1969)
3.8449	4.7688	0.057	0.184	0.165	
3.9016	4.1552	0.033	0.100	0.108	Present Work
3.8926	4.1767	0.030	0.105	0.110	Present Work[a]
3.8349	4.3028	0.042	0.134	0.134	DFT-GGA(Saghi-Szabo, Cohen, & Krakauer, 1998)
3.9053	4.1514	0.049	0.125	0.130	DFT-LDA[b] (Saghi-Szabo et al., 1998)
					DFT-LDA[c] (Garcia & Vanderbilt, 1996)

[a] Experimental volume with fixed lattice constants
[b] Constant volume, all-electron basis set
[c] Constant volume with fixed lattice constants

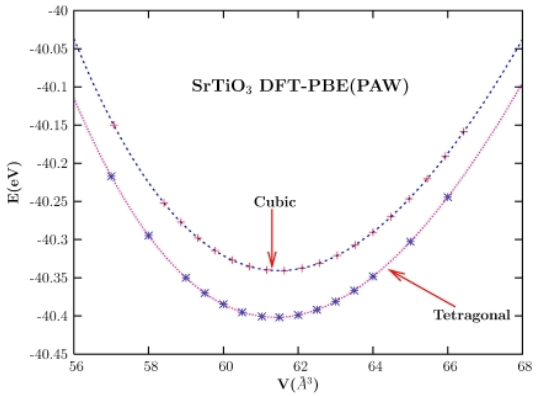

Figure 3: Energy as a function of volume for the cubic and tetragonal phases of $SrTiO_3$ from ab-initio calculations using DFT-PBE. Curves stand for the EOS fitting. Tetragonal structure results were scaled back to one molecular unit formula, Z=1.

Suard, & Ratuszna, 2004). At high temperatures $AgNbO_3$ has cubic structure with Pm3m point group symmetry. At T=630°C, cubic to tetragonal (P4/mbm) phase transition takes place. In a previous experimental study, tetragonal phase was reported to have I4/mcm point group symmetry (Ratuszna, Pawluk, & Kania, 2003). Also, the transition from tetragonal to orthorhombic phase is not clear in recent experimental studies. Sciau *et al.* (Sciau et al., 2004) reported the high temperature phase transition possibly from tetragonal P4/mbm to orthorhombic Cmcm to occur at 372 °C by using neutron diffraction studies, whereas Ratuszna *et al.* (Ratuszna et al., 2003) reported the tetragonal I4/mcm to orthorhombic Pmmn phase transition to occur at 388 °C by using X-ray diffraction data.

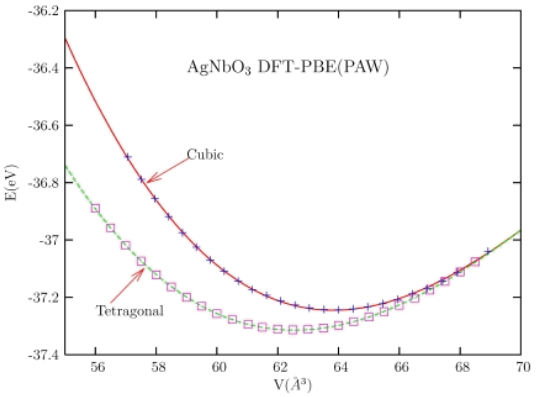

Figure 4: Energy as a function of volume for the cubic and tetragonal phases of $AgNbO_3$ from ab-initio calculations using DFT-PBE. Curves stand for the EOS fitting. Tetragonal structure results were scaled back to one molecular unit formula, Z=1.

At 300 °C, orthorhombic to monoclinic (Pbcm) phase transition was reported to occur (Sciau et al., 2004) while Ratuszna *et. al.* reported phase transitions to a monoclinic (Pmna) phase at 327 °C and a monoclinic ($B2_1/m$) phase at 27 °C. The different conclusions reached from these two

experimentals present a challenge to test these structures by quantum mechanics. In Figure 4, energy-volume behavior of cubic and tetragonal (P4/mbm) is plotted.

Equation of state results for $PbTiO_3$, $SrTiO_3$ and $AgNbO_3$ are tabulated for cubic and tetragonal structures in Table 9. Bulk modulus result of this work for cubic $PbTiO_3$ is the closest one to experimental result among the results of other theoretical calculations. But equilibrium volume of the tetragonal structure is 11.4% greater than experimental volume. For tetragonal $SrTiO_3$ and cubic and tetragonal $AgNbO_3$, there is no experimental and theoretical work to compare with.

3.2 *Density Functional Studies on the Equation of State of Alloy Structures*

To study the equations of state and stability of ABO_3 alloys, we constructed supercells by replicating the unit cells $2\times2\times2$ times to create supercell models with 40 atoms for calculations. This enables us to study the composition dependence in steps of 0.125. We conducted calculations on $Pb_xBa_{8-x}(TiO_3)_8$ and $Sr_xBa_{8-x}(TiO_3)_8$ (where x = 1, ..., 7). For each alloy concentration, the possible structural arrangements have been also considered to find the energetically favorable arrangement. At each alloy concentration and structural arrangement, various single point energy calculations have been performed by changing the volume in order to get the EOS. Energy-volume behavior are plotted in Figure 5 and Figure 6 for $Pb_xBa_{8-x}(TiO_3)_8$and $Sr_xBa_{8-x}(TiO_3)_8$, respectively. The EOS results are tabulated in Table 10 and Table 11.

3.2.1 *Band Structure of ABO_3 ferroelectrics*

Band structure of $BaTiO_3$ has been extensively studied since it supplies useful information in understanding the nature of ferroelectricity. Electronic energy band structures of cubic and tetragonal $BaTiO_3$ are shown in Figure 7 and Figure 8, respectively. Calculations have been performed at experimental lattice constants to compare with available data. Form of the energy bands seems more likely to be in the form of the bands of ionic materials: well separated. Each band is marked

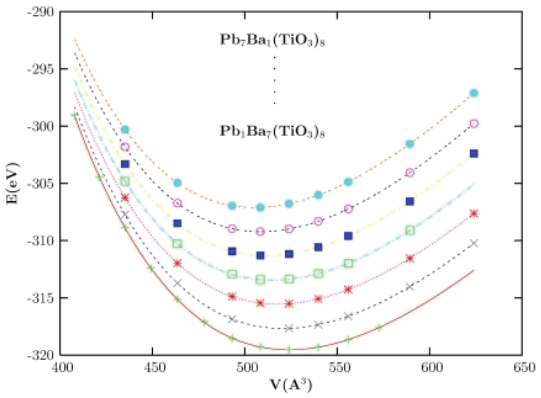

Figure 5: Energy as a function of volume for the cubic $Pb_xBa_{8-x}(TiO_3)_8$ from ab-initio calculations using DFT-PBE for 2x2x2 supercell. x stands for alloy concentration of Pb which changes from 1 to 7. Curves stand for the EOS fitting.

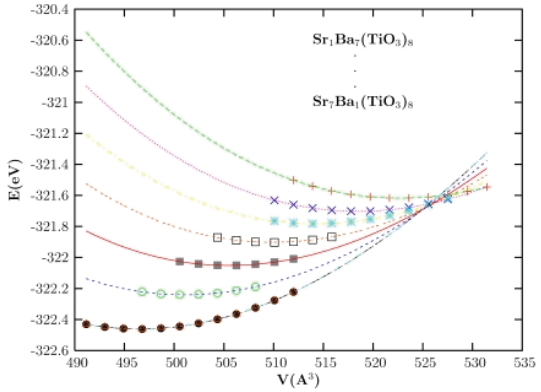

Figure 6: Energy as a function of volume for the cubic $Sr_xBa_{8-x}(TiO_3)_8$ from ab-initio calculations using DFT-PBE for 2x2x2 supercell. x stands for alloy concentration of Sr which changes from 1 to 7. Curves stand for the EOS fitting.

with the dominant character of atomic orbital that mainly composes the particular energy state in the solid.

Although the system is mainly ionic, there is some covalent character for some bands which is crucial for ferroelectric nature of the material (Cohen, 1992; Cohen & Krakauer, 1992; Ghosez, Gonze et al., 1999). Hybridization between O 2p and Ti

Table 10: EOS parameters of $PbTiO_3$, $SrTiO_3$, $AgNbO_3$ for the cubic and tetragonal structures: volume (lattice constant), cohesive energy, B, bulk modulus and B', pressure derivative of bulk modulus. Results for $SrTiO_3$ and $AgNbO_3$ were scaled back to one molecular unit formula, Z=1.

		$V_0(A^3)$	E_{COH}(eV)	B(GPa)	B'	Reference
$PbTiO_3$	Cubic	62.57		144 (Li,		Exp.(Hellwege &
		62.78	38.05	Grimsditch,	4.50	Hellwege, 1969)
		59.23		Foster, &		Present Work
		58.54		Cha, 1996)		DFT-LDA(Fu &
		58.82		172.57		Gülseren, 2002)
		58.82		212		DFT-LDA(Waghmare
		62.10		203		& Rabe, 1997)
		62.10		215		DFT-LDA Ref.2 of
				209		(Waghmare & Rabe,
				213		1997)
				217		DFT-LDA Ref.4 of
						(Waghmare & Rabe,
						1997)
						DFT-GGA(Piskunov et
						al., 2004)
						DFT-GGA(Piskunov et
						al., 2004)
	Tetragonal	63.28				Exp.(Hellwege &
		70.50	38.24	44.07		Hellwege, 1969)
		59.62				Present Work
						DFT(Cooper, Grinberg,
						& Rappe, 2003)
$SrTiO_3$	Cubic	59.55		174		Exp.(Hellwege &
		59.46	31.7			Hellwege, 1969)
				183.0		Exp.(Weyrich & Siems,
		61.49	40.34	168.6	4.39	1985)
		60.34		190		Exp.(Fischer, Wang, &
		60.74	28.2	202.6		Karato, 1993)
		58.00	39.2	198.4		Present Work
		61.49	30.7	179.1		DFT-LDA(Lasota,
		61.34	33.9	172.5		Wang, Yu, & Krakauer,
		61.63		170		1997)
		61.16		171		Hartree-Fock(Ricci,
						Bano, Pacchioni, &
						Illas, 2003)
						DFT-LDA(Ricci et al.,
						2003)
						DFT-B3LYP(Ricci et
						al., 2003)
						DFT-PW91(Ricci et al.,
						2003)
						DFT-GGA(Piskunov et
						al., 2004)
						DFT-PBE(Piskunov et
						al., 2004)
	Tetragonal	61.39	40.40	165.7	4.25	Present Work
$AgNbO_3$	Cubic	63.09				Exp.(Sciau et al., 2004)

Table 11: : EOS parameters of alloy $Pb_xBa_{8-x}(TiO_3)_8$ for the 2×2×2 supercell cubic structure: lattice constant, cohesive energy, B, bulk modulus and B' , pressure derivative of bulk modulus for 5 atom unit cell. Here x stands for alloy concentration of Pb which changes from 1 to 7.

Alloy	a(A)	E_{COH}(eV)	B(GPa)	B'
$Pb_7Ba_1(TiO_3)_8$	3.98282	38.3895	170.3485	4.49
$Pb_6Ba_2(TiO_3)_8$	3.99088	38.6520	168.9422	4.50
$Pb_5Ba_3(TiO_3)_8$	3.99893	38.9144	167.4709	4.49
$Pb_4Ba_4(TiO_3)_8$	4.00698	39.1826	165.8621	4.53
$Pb_3Ba_5(TiO_3)_8$	4.01472	39.4429	164.8040	4.54
$Pb_2Ba_6(TiO_3)_8$	4.02274	39.7103	163.4699	4.51
$Pb_1Ba_7(TiO_3)_8$	4.03067	39.9421	161.7157	4.57

Table 12: : EOS parameters of alloy $Sr_xBa_{8-x}(TiO_3)_8$ for the 2×2×2 supercell cubic structure: lattice constant, cohesive energy, B, bulk modulus and B' , pressure derivative of bulk modulus for 5 atom unit cell.

Alloy	A(A)	E_{COH}(eV)	B(GPa)	B'
$Sr_7Ba_1(TiO_3)_8$	3.95925	40.3078	167.3988	4.37
$Sr_6Ba_2(TiO_3)_8$	3.97126	40.2801	166.4377	4.23
$Sr_5Ba_3(TiO_3)_8$	3.98304	40.2565	165.5737	4.54
$Sr_4Ba_4(TiO_3)_8$	3.99453	40.2379	164.4681	4.37
$Sr_3Ba_5(TiO_3)_8$	4.00585	40.2229	163.6316	4.47
$Sr_2Ba_6(TiO_3)_8$	4.01687	40.2129	162.7155	4.51
$Sr_1Ba_7(TiO_3)_8$	4.02776	40.2023	161.8789	4.11

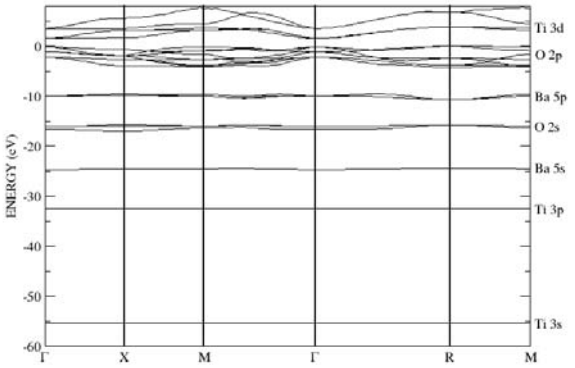

Figure 7: Band structure for $BaTiO_3$ in the experimental cubic structure. Names of the atomic orbitals which mainly compose particular energy state are written.

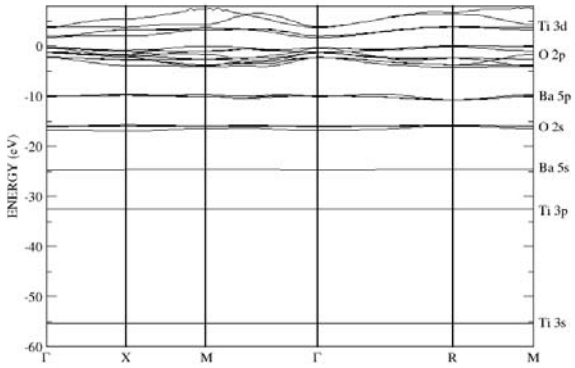

Figure 8: Band structure for $BaTiO_3$ in the experimental tetragonal structure. Names of the atomic orbitals which mainly compose particular energy state are written.

3d orbitals causes four electrons of the Ti 3d orbital partly delocalized. Therefore, O 2p bands gain some admixture of Ti 3d character. This feature was clearly identified from the overlap integrals in the early Linear Combination of Atomic Orbital (LCAO) band structure calculations on ABO_3 compounds (Kahn & Leyendecker, 1964; Mattheiss, 1972). It was often accepted as an essential feature to explain the ferroelectricity in these materials (Migoni, Bilz, & Bauerle, 1976). Also, it was also shown that only the cubic structure was stable without Ti-O hybridization in the titanates (Cohen & Krakauer, 1992).

For $BaTiO_3$, calculated band gaps in cubic and

tetragonal structures are indirect (R → Γ). Indirect energy gaps are 1.55 and 1.59 eV in cubic and tetragonal structures, respectively. Direct band-gaps (Γ → Γ) are 1.66 and 1.94 eV. Results of energy gaps calculated from DFT, generally underestimate 30 to 50% sometimes 100% of the experimental values. Also, comparison can not be made with experiment because there is a well-known experimental problem in ferroelectric materials (Wemple, 1970). Absorption coefficient increases exponentially with increasing photon energy so no defined band-gap can be extracted from absorption measurements (Urbach-rule behavior). Wemple (Wemple, 1970) estimated a realistic value of 3.2 eV.

Comparison between the cubic and tetragonal structures of $BaTiO_3$ is shown in Figure 9 for top valence bands and lowest conduction bands. Top of the valence band is shifted to zero energy for convenience. Top valence bands (Ti 3d character) of tetragonal structure are lowered down in energy towards O 2p states at Γ point. This lowering in energy can be easily attributed to hybridization of these states due to ferroelectric transition.

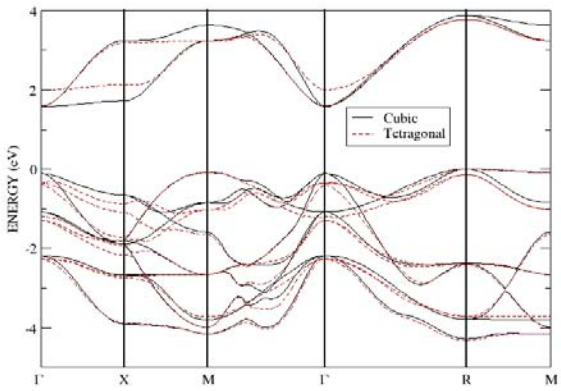

Figure 9: Band structure of $BaTiO_3$ for the top valence and bottom conduction bands in the experimental structure cubic tetragonal structures.

Despite having the same ferroelectric behavior at high temperatures with $BaTiO_3$, $PbTiO_3$ has a different electronic structure. Electronic band structure of experimental cubic $PbTiO_3$ is shown in Figure 10. Energy level of Pb 6s is closer to O 2p bands than as Ba 5p bands being closer to O

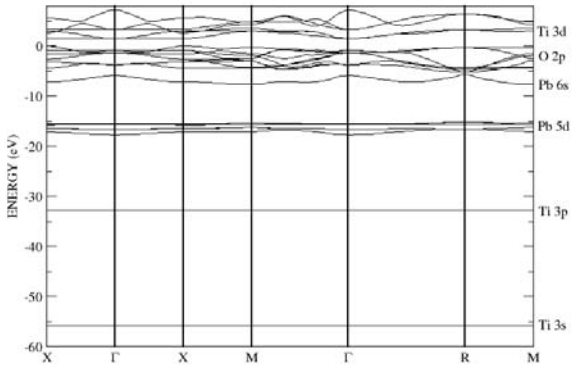

Figure 10: Band structure for $PbTiO_3$ in the experimental cubic structure. Names of the atomic orbital which mainly composes particular energy state are written.

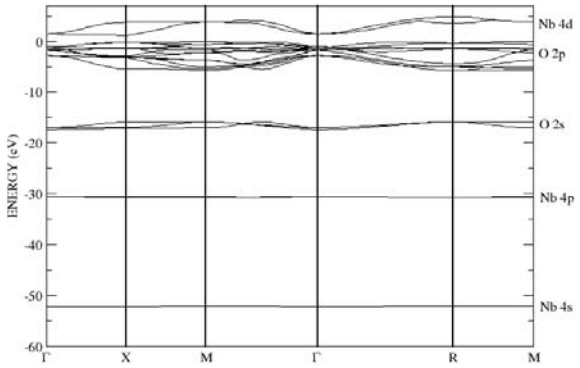

Figure 11: Band structure for $AgNbO_3$ in the experimental cubic structure. Names of the atomic orbital which mainly composes particular energy state are written.

2p bands in $BaTiO_3$. Consequently, this interaction between Pb 6s and O 2p increases the hybridization of O 2p and Ti 3d states (Cohen & Krakauer, 1992). This covalency is clarified by a recent experimental study (Kuroiwa, Aoyagi, & Sawada, 2001). Indirect band gap (X → Γ) is 1.43 eV while direct band gap is 2.31 eV. Experimental value is 3.4 eV (Peng, Chang, & Desu, 1992).

In Figure 11, electronic energy bands are plotted for cubic $AgNbO_3$. There are subtle differences with the electronic structure of $BaTiO_3$. First of all, $AgNbO_3$ is a Ag=+1, Nb=+5 ionic compound while $BaTiO_3$ is a Ba=+2 Ti=+4. Secondly, the minimum of valence band lies in M-point for $AgNbO_3$. Finally, there is hybridization between

both Nb 4d and O 2p and Ag 4d and O 2p orbitals as well. Indirect energy gap ($M \rightarrow \Gamma$) is calculated for $AgNbO_3$ as 1.41 eV while the direct band gap is 2.41 eV. Experimental energy gap was reported to be 2.8 eV (Kato, Kobayashi, & Kudo, 2002).

3.2.2 *Born Effective Charges and Phonon Dispersion Relation*

Definition of atomic charge for atoms in molecules or solids is not well defined. There are various kinds of charges in order to describe the ionicity or polarity of chemical bonds (Meister & Schwarz, 1994): Mulliken charge, Hirshfeld charge, Bader charge . All of them have their own convention.

On the other hand, Born effective charge, Z^* is a fundamental quantities which shows the coupling between lattice displacements and electrostatic fields in insulators. It is also known as transverse or dynamic effective charges. It is related to the change of polarization with respect to atomic displacements (King-Smith & Vanderbilt, 1993). Change of polarization can be experimentally measured and can give a well-defined character to Z^*.

Born effective charge is also important in terms of theoretical investigation of ferroelectric materials. Ferroelectric transitions take place from the competition of long-range Coulomb interactions and short-range forces. Thus, long-range Coulomb interactions are the cause of the split between the frequencies of the longitudinal optical (LO) and transverse optical (TO) phonons (Lyddane, Sachs, & Teller, 1941). The tool to monitor the long-range Coulomb interaction for this splitting is the Born effective charge.

Axe (Axe, 1967) proposed experimentally an estimation of Z^* for ABO_3 compounds. He suggested anomalous effective charges. Harrison (Harrison, 1980) also suggested from empirical studies that amplitude of Born effective charges should deviate from static ionic charges. Since the recent advances in ab initio techniques, Z^* has been accessible from theoretical calculations by using perturbation theory (Gonze et al., 1992; Lee et al., 1994) or finite difference of polarization (King-Smith & Vanderbilt, 1993). With the results obtained from first-principles calculations (Ghosez & Gonze, 2000; Ghosez, Gonze, Lambin, & Michenaud, 1995; Ghosez, Michenaud, & Gonze, 1998; Veithen, Gonze, & Ghosez, 2002; Zhong, King-Smith, & Vanderbilt, 1994), Z^* was confirmed to be anomalously large, sometimes as much as twice of the nominal ionic charge.

In Table 12, Born effective charges and optical dielectric constant for $BaTiO_3$, $PbTiO_3$, $SrTiO_3$, $AgNbO_3$ and $AgTaO_3$ are presented. Calculations have been performed at experimental lattice constants and at optimized zero-pressure states which have lattice constants as 4.052, 3.998, 3.967, 4.008 and 3.928 Angstrom for $BaTiO_3$, $PbTiO_3$, $SrTiO_3$, $AgNbO_3$ and $AgTaO_3$, respectively. For $BaTiO_3$, Ba and Ti atoms have isotropic charge tensor, while O atoms have perpendicular, $O_\perp$ and parallel, $O_\parallel$ charge tensor components to Ti-O bonding. Born effective charges of Ti and $O_\parallel$ are quite larger than their nominal values (+4 for Ti and -2 for O). Essentially, these anomalous charges reveal the mixed ionic and covalent character of the bond. Optical dielectric constant (calculated at experimental lattice constant) 6.80 is 26% larger than the experimental value 5.40 (as expected within DFT). This difference in optical dielectric coefficient will affect the value of the highest longitudinal optic mode. After replacing the theoretical dielectric constant with the experimental value, frequency of the highest longitudinal optic (LO) mode changes from 82.87 to 89.32 meV. Experimental value of this highest mode is 95.73 meV. By using the experimental dielectric constant, Ph. Ghosez *et al.* (Ghosez, Gonze et al., 1998) shifted their highest (LO) from 78.23 to 86.29 meV.

In Table 12, for $BaTiO_3$, at experimental volume, Ba and Ti charges are 2.74 and 7.85, respectively. But at zero pressure volume, significant changes in Z_{Ti} and $Z_{O\parallel}$ are observed due to increase of Ti-O bond distance. Results are in good agreement with the other theoretical works.

Changes on Z_{Ti} and $Z_{O\parallel}$ are surprisingly large, even twice of their static value. This anomalous contribution can be attributed to a large dynamical contribution superimposed to the static charge of the system. Within Harrison's...(Harrison,

Table 13: Born effective charges and optical dielectric constant of ABO_3 (A=Ba, Pb, Ag B=Ti, Nb, Ta) in the cubic structure.

	Z_A	Z_B	$O_{\parallel}$	$O_{\perp}$	ε_{∞}	Reference
$BaTiO_3$	2.9	6.7	-4.8	-2.4	5.40[a]	Exp.(Axe, 1967)
					5.24[b]	Exp.(Mitsumi et al., 1981)
	2.71	7.80	-	-	7.28	Present Work
			6.21	2.15		(P=0 GPa)
	2.74	7.45			6.80	Present Work
			-	-		a=4.00 A
	2.74	7.32	5.74	2.14	6.75	DFT-LDA(Ghosez, Gonze et al., 1998)
	2.75	7.16				DFT-LDA(Zhong et al., 1994)
	2.77	4.83	-	-		MD (P-QEq)(Zhang, 2004)
	1.93	6.45	5.78	2.14		MD(Tinte, Stachiotti, Sepliarsky, Migoni,
			-	-		& Rodriguez, 1999)
			5.69	2.11		(Dynamic Shell Model)
			-	-		
			4.76	1.42		
			-	-2.3		
			3.79			
$PbTiO_3$					8.64[b]	Exp.(Mitsumi et al., 1981)
	3.89	7.68	-	-	9.29	Present Work
			6.36	2.60		(P=0 GPa)
	3.92	7.36			8.82	Present Work
			-	-		(a=3.97 Å)
	3.90	7.06	5.94	3.62		DFT-LDA(Zhong et al., 1994)
			-	-		
			5.83	2.56		
$SrTiO_3$	2.4	7.0	-5.8	-1.8		Exp.(Axe, 1967)
					5.18[b]	Exp.(Mitsumi et al., 1981)
	2.55	7.73	-	-	6.85	Present Work
			6.17	2.05		(P=0 GPa)
	2.56	7.26				DFT-LDA(Ghosez, Michenaud et al.,
	2.54	7.12	-	-		1998)
	2.55	7.56	5.73	2.15		DFT-LDA(Zhong et al., 1994)
			-	-2.0		(Lasota et al., 1997)
			5.66	-		
			-	2.12		
			5.92			
$AgNbO_3$	1.60	10.04	-	-	8.51	Present Work
			8.17	1.90		(P=0 GPa)
	1.61	10.08			8.38	Present Work
			-	-		(a=3.98 Å)
	1.04	10.06	7.71	1.85		DFT(Prosandeev, 2005)
			-	-		
			6.33	2.39		
$AgTaO_3$	1.56	8.62	-	-	6.24	Present Work
			6.52	1.83		(P=0 GPa)

[a] ε_{∞} was obtained by extrapolating to zero frequency index of refraction measurements (Burns & Dacol, 1982).

[b] Experimental values for $\varepsilon_{\infty}(0)$ observed in the visible light range (Mitsumi et al., 1981) extrapolated to the optical $w = 0$ limit using dispersion relation $\varepsilon - 1 = C/(w_0^2 - w^2)$, where C and w_0 are constants.

1980) Bond Orbital Model (BOM), ABO_3 compounds are described as mixed ionic-covalent compounds. In $BaTiO_3$, this hybridization is also a well known property of the system from experiment (Nemoshkalenko & Timoshevskii, 1985), tight-binding model (Harrison, 1980) and LCAO calculations (Michel-Calendini, Chermette, & Weber, 1980). Cohen (Cohen, 1992) also stated from first principles that O 2p-Ti 3d hybridization is an essential feature of ABO_3 type ferroelectric compounds. Posternak, Resta and Baldereschi (Posternak, Resta, & Baldereschi, 1994) showed for $KNbO_3$ that the anomalous contributions disappear when the interaction between O 2p and Nb 4d is artificially suppressed.

In order to clarify the microscopic origin of the anomalous contributions, band-by-band decomposition of Born Effective charges are calculated within the content of the recent theory of polarization (King-Smith & Vanderbilt, 1993; Vanderbilt & King-Smith, 1993). As expressed by Ghosez, Michenaud and Gonze (Ghosez, Michenaud et al., 1998), "*the true quantum mechanical electronic system can be considered as an effective classical system of quantized point charges, located at the centers of gravity associated with the occupied Wannier functions in each unit cell*." In these terms, the important quantity is the displacement of valence charge center, not reproducing all the features of valence charge distribution. The anomalous charge associated to a particular band for a given ion reflects how the center of the Wannier function of this band moves with respect to the ion. In a purely ionic material, each band would be composed of a single nonhybridized orbital and Wannier center of each band would be centered on a given atom. In the absence of any hybridization, when an atom is displaced, the Wannier center of bands centered on the moving atom would remain centered on it, while the position of the center of gravity of the other bands would remain unaffected. The contributions of these two kinds of bands to Z would therefore be -2 and 0, respectively.

In a real material, anomalous charge contribution to reference value is an additional part in absence of any hybridization: it shows how the center of the Wannier center of band $m$is displaced relatively to the atoms when sublattice of atoms κmoves.

Considering each band as a combination of atomic orbitals, such a displacement of the Wannier center of a band with respect to its reference position must be attributed to hybridization effects. When the interacting orbitals are located on different atoms, dynamical changes of hybridization can be visualized as transfers of charge (off-site hybridization). If the interacting orbitals are on the same atom (on-site hybridization), this is much like a polarizability.

Band-by-band decomposition of dynamical charges for $BaTiO_3$ is tabulated in Table 14. First line is the charge of the nucleus and core electrons defined by the pseudopotential. Other contributions come from the valence electron levels. The atomic orbitals which mainly makes up the particular energy state are also identified from density of states calculations (Figure 7).

The main anomalous charge for Ti is localized on O 2p states (+3.07). This charge corresponds to a displacement of the Wannier center of the O 2p bands in the opposite direction (towards) to the displacement of the Ti atom. Considering the hybridization between O 2p and Ti 3d states, this is the shortening of the Ti-O bond with a transfer of electron from O to Ti by dynamical changes of hybridization. There are small but non-negligible contributions coming from Ti 3p (-0.16), O 2s (+0.22) and Ba 5p (0.29). The positive anomalous charges correspond to a displacement of the center of Wannier function of the O and Ba bands in the direction of closest Ti atom when this atom has moved.

Ba has global anomalous effective charge (+0.74), which is less than the anomalous charge of Ti. This feature was at first attributed to the ionic character of Ba. However, anomalous charges of O 2s (+0.64) and O 2p (+1.26) are not small at all. Other anomalous charges of Ba 5s (-0.08) and Ba 5p (-1.11) can not compensate these contributions. Therefore, these anomalous charges reveal that there is also hybridization between Ba and O atoms. This conclusion has also been confirmed by experiments (Hud-

son, Kurtz, Robey, Temple, & Stockbauer, 1993; Nemoshkalenko & Timoshevskii, 1985), LCAO calculations (Michel-Calendini et al., 1980; Pertosa & Michel-Calendini, 1978), and DFT computations (Weyrich & Siems, 1985). It is important to mention that unlike the hybridization between Ti 3d and O 2p orbitals, the mechanism here is restricted only to occupied states. Also, it must be stated that amplitude of the anomalous contributions to Z is not related to amplitude of hybridization but to the rate of change of these hybridizations under atomic displacements. In $BaTiO_3$, it is clear that the Ba 5p contribution to the O 2p bands is smaller than the contribution from the Ti 3d orbitals (Cohen, 1992; Weyrich & Siems, 1985). However, with the help of Born effective charge, it is possible to get even relatively weak covalent character.

For oxygen, $Z_{O_\parallel}$ and $Z_{O_\perp}$ are defined for a displacement along Ti and Ba atoms, respectively. Qualitatively, $Z_{O_\parallel}$ can be associated with Z_{Ti} and $Z_{O_\perp}$ withZ_{Ba}. The O 2p anomalous contributions to Ti and $O_\parallel$ do not exactly compensate. Moreover, O 2p contribution to Z_{Ba} does not only come from $O_\perp$ but has equivalent contributions from$O_\parallel$.

To summarize, the mixed ionic-covalent character of $BaTiO_3$ has been clarified by band-by-band decomposition of Born effective charges. In addition to well-known covalent character of Ti-O bond, Ba-O bond also has a covalent nature. Also, presence of a large anomalous charge requires a modification of the interactions between occupied and unoccupied electronic state. Interactions between two occupied electronic states result with a compensated charge and do not modify the global value of Z.

Anomalous charge contributions for different bands of $BaTiO_3$ are in good agreement with other DFT results (Ghosez & Gonze, 2000; Ghosez et al., 1995; Ghosez, Michenaud et al., 1998).

For $AgNbO_3$, band-by-band decomposition of Born effective charges is tabulated in Table 16. Total Z for Nb is twice (+10.08) of the nominal charge (+5). For$O_\parallel$, Z is almost four times (-7.71) greater than its nominal value (-2.0).

Main anomalous charge for Nb is localized on O 2p states (+4.88). Like in the case of $BaTiO_3$ for Ti atom, this charge corresponds to a displacement of the Wannier center of the O 2p bands towards to the displacement of the Nb atom. There are small contributions coming from O 2s (+0.61) and Nb 4p (-0.38) bands.

Ag seems to be the ionic component of this ferroelectric system. But with a total anomalous charge of (+0.61), contribution from O 2s band (+0.12) and compensating contribution from O 2p band (-9.52), Ag 4d and O 2p orbitals have hybridization. It is worth to mention that top valence bands have O 2p character although they have also hidden Ag 4d character.

For oxygen, $Z_{O_\parallel}$ and $Z_{O_\perp}$ are defined for a displacement along Nb and Ag atoms, respectively. Qualitatively, $Z_{O_\parallel}$ can be associated with Z_{Nb} and $Z_{O_\perp}$ withZ_{Ag}. The O 2p anomalous contributions to Nb and $O_\parallel$ do not exactly compensate. Moreover, O 2p contribution to Z_{Ag} does not only come from $O_\perp$ but has equivalent contributions from$O_\parallel$. Generally speaking, transfer of charges is not restricted to a particular bond, but it is a rather complex mechanism that must be treated as a whole.

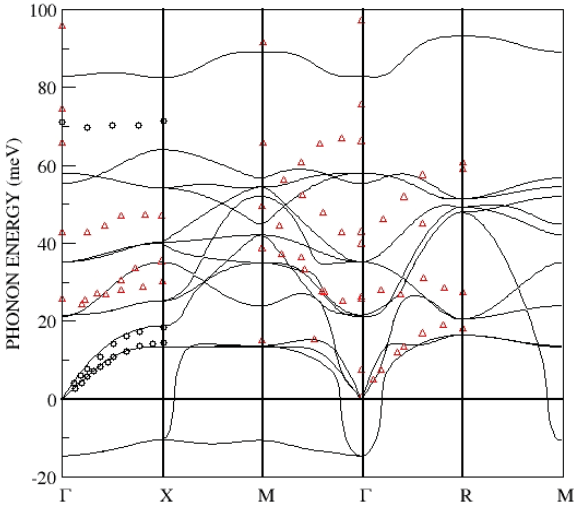

Figure 12: Phonon dispersion curves of $BaTiO_3$ at experimental lattice constant. Theoretical result shows an agreement with the experimental data: (◯) (Shirane, Frazer, Minkiewicz, & Leake, 1967), (△) (Jannot, Escribe-Filippini, & Bouillot, 1984).

Table 14: Band-by-band decomposition of Z in the experimental volume of cubic $BaTiO_3$. First line is the charge of the nucleus and core electrons defined in the pseudopotential. Contributions have been separated into a reference value and an anomalous charge.

Band	Z_{Ba}	Z_{Ti}	$Z_{O_\parallel}$	$Z_{O_\perp}$
Core	10.00	12.00	6.00	6.00
Ti 3s	0 +0.01	-2 -2.03	0 +0.01	0 02 -0.01
Ti 3p	0 +0.02	-6 -6.16	0 +0.160 +0.01	0 +0.01
Ba 5s	-2 -2.08	0 +0.05	-2 -2.47	-2 -2.20
O 2s	0 +0.64	0 +0.22	0 -0.08	0 +0.44
Ba 5p	-6 -7.11	0 +0.29	-6 -9.42	-6 -6.33
O 2p	0 +1.26	0 +3.07		
Total	2.74	7.44	-5.79	-2.07

Table 15: Band-by-band decomposition of Z in the experimental volume of cubic $PbTiO_3$. First line is the charge of the nucleus and core electrons defined in the pseudopotential. Contributions have been separated into a reference value and an anomalous charge.

Band	Z_{Pb}	Z_{Ti}	$Z_{O_\parallel}$	$Z_{O_\perp}$
Core	14.00	12.00	6.00	6.00
Ti 3s	0 +0.01	-2 -2.03	0 +0.02	0 +0.00
Ti 3p	0 +0.02	-6 -6.17	0 +0.18	0 -0.02
Pb 5d	-10 -9.86	0 +0.33	0 -2.51	0 -1.98
Pb 6s	-2 -3.40	0 +0.56	-2 -0.24	-2 -0.53
O 2p	+0 +3.15	0 +2.67	-6 -9.39	-6 -7.09
Total	3.92	7.36	-5.94	-3.62

Table 16: Band-by-band decomposition of Z in the experimental volume of cubic $AgNbO_3$. First line is the charge of the nucleus and core electrons defined in the pseudopotential. Contributions have been separated into a reference value and an anomalous charge.

Band	Z_{Ag}	Z_{Nb}	$Z_{O_\parallel}$	$Z_{O_\perp}$
Core	+11.00	+13.00	+6.00	+6.00
Nb 4s	0 +0.00	-2 -2.03	0 +0.03	0 0.00
Nb 4p	0 +0.01	-6 -6.38	0 +0.46	0 -0.04
O 2s	0 +0.12	0 +0.61	-2 -2.98	-2 -1.86
O 2p	0 -9.52	0 +4.88	-6 -11.22	-6 -5.95
Total	1.61	10.08	-7.71	-1.85

Phonon band structure of $BaTiO_3$ is plotted in Figure 12 along high symmetry lines Γ-X-M-Γ-R-M by using 4x4x4 Monkhorst-Pack(MP) grid. Full phonon curve is also calculated with 8x8x8 MP grid. Change observed in these plots is in the magnitude of softmodes. These modes seem to be more unstable in 8x8x8 grid. Soft-mode frequency is $14.5i$ and $21.3i$in 4x4x4 and 8x8x8 MP grids, respectively. Stable modes are relatively unaffected. Negative frequency in the plot shows the imaginary frequency associated with unstable modes. However, experimentally observed frequencies have real values while theoretical calculations show unstable phonon modes which are the driving force for ferroelectric phase transitions. At Γ point, two of the transverse optic modes are unstable. Eigenvectors associated with these modes are $\gamma(Ba) = 0.009$, $\gamma(Ti) = 0.360$, $\gamma(O_2) = -0.296$ and $\gamma(O_1 = O_3) = -0.177$ Å (Eigenvectors are normalized, $\langle\gamma|\gamma\rangle = 1$and converted to angstrom). As discussed by Ph. Ghosez *et al.* (Ghosez, Gonze et al., 1998), along Γ-M and X-M lines, one of these two stabilizes. Finally, all of the

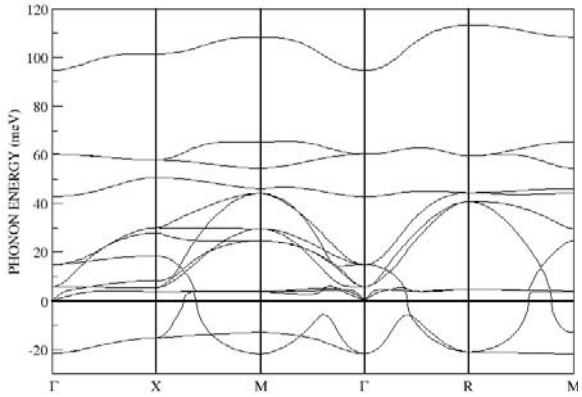

Figure 13: Phonon band structure of $AgNbO_3$ at experimental lattice constant.

modes become stable in the vicinity of R-point. At high symmetry point M(0.5, 0.5,0), eigenvectors show that unstable mode is polarized along the z-direction[$\gamma(\mathrm{Ti_z}) = -0.512$Å and $\gamma(\mathrm{O_{1,z}}) = 0.133$ Å]. Frequencies at high symmetry points are reported in Table 17.

Phonon band structure of $BaTiO_3$ is similar to $KNbO_3$ phonon curves (Yu & Krakauer, 1995). Yu *et. al. (Yu & Krakauer, 1995)* reported that correlated atomic displacements along $< 001 >$ chain are at the origin of ferroelectric instability for $KNbO_3$. For $BaTiO_3$, at M-point, there is a single unstable mode polarized along the z-axis. At his wave vector (q_z=0), Ti and O_1 atoms will be displaced along an infinite $< 001 >$ chain. Going from M to R, the effect of this displacement will gradually disappear. The thickness of the instability region between M and R points corresponds to a minimum correlation length where the phonons become stable. This correlation length of 18 Å is in agreement with the finding of 16 Å of Ghosez *et. al. (Ghosez, Gonze et al., 1998).*

Chain instability can be also viewed from interatomic force constants (IFC) along Ti-O chain. The IFC, $C_\alpha(\kappa,\kappa')$ can be defined as the force $F_\alpha(\kappa)$ induced on atom κ by the displacement $\Delta\tau_\beta(\kappa')$ of atom κ' by: $F_\alpha(\kappa) = -C_{\alpha,\beta}(\kappa,\kappa').\Delta\tau_\beta(\kappa')$. The results are tabulated for a reference Ti atom (0.5, 0.5, 0.5) along Ti-O chain in Table 18. Self-force of Ti atom is large and positive (+0.16887 Ha/Bohr^2). Surprisingly, the longitudinal IFC with the first neighbor O atom is very small (-0.00234). From the analysis of the dipole-dipole (DD) and short-range (SR) forces (Gonze et al., 1994) contributions, destabilizing DD interaction is large enough to compensate the SR forces. Thus, the displacement of Ti atom against O is a result of this compensation. Therefore, this small total IFC is a result of decoupling of Ti and O displacements. But this small decoupling (relatively weak coupling) plays an important role in the appearance of the linear ferroelectric instability. DD forces induced on the next Ti atom is negative pointing out a coupling (-0.06979 Ha/Bohr^2) with the addition of SR forces. Contrary to longitudinal forces, the transverse force on the first Ti neighbor is very small (+0.00919) confirming the small correlation of the displacements from chain to chain.

Phonon band structure of $AgNbO_3$ shows highly unstable modes (Figure 13). There are two unstable transverse optic modes at Γpoint. Eigenvectors associated with these modes are $\gamma(\mathrm{Ag}) = 0.053$, $\gamma(\mathrm{Nb}) = 0.268$, $\gamma(\mathrm{O_2}) = -0.244$ and $\gamma(\mathrm{O_1} = \mathrm{O_3}) = -0.270$ Å. Along X-M line, one of the unstable modes become stable but another mode becomes unstable shortly. Through the Γ-R line, a third mode becomes unstable. Interestingly, along R-M line, two of the three unstable modes become stable but close to M point, the number of unstable modes becomes two. Frequencies at high symmetry points are reported in Table 19.

Comparison of the IFC of $AgNbO_3$ (Table 20) and $BaTiO_3$ shows similar behavior but the IFC's of $AgNbO_3$ is larger. From point of view of chain instability, longitudinal IFC of first neighbor O atom is small (-0.002868 Ha/Bohr^2) with respect to first nearest Nb total IFC(-0.10362 Ha/Bohr^2). Longitudinal DD force on first neighbor O atom is large enough to compensate the SR force (relatively weak coupling). Cotrary to longitudinal forces, the transverse component of the force on the first Nb neighbor is very small (+0.01419 Ha/Bohr^2) confirming the small correlation of the displacements from chain to chain.

Table 17: Computed phonon frequencies (meV) of cubic $BaTiO_3$ at experimental lattice constant of 4.0 A, atΓ, X, M and R. Second frequency set was calculated by using DFT-LDA at experimental lattice constant by Ph. Ghosez et al (Ghosez, Gonze et al., 1998).

q-point	Label	Freq. Pres.Work	Label	Freq. Pres.Work	Label	Freq. (Ghosez, Gonze et al., 1998)	Label	Freq. (Ghosez, Gonze et al., 1998)
Γ	Γ_{15}(TO) Γ_{15}(A) Γ_{15}(LO) Γ_{15}(TO)	14.53i 0 21.20 21.63	Γ_{25} Γ_{15}(LO) Γ_{15}(TO) Γ_{15}(LO)	35.21 55.34 58.02 82.87	Γ_{15}(TO) Γ_{15}(A) Γ_{15}(LO) Γ_{15}(TO)	27.15i 0 19.71 20.58	Γ_{25} Γ_{15}(LO) Γ_{15}(TO) Γ_{15}(LO)	34.84 55.17 56.16 78.23
X	X_5 $X_{5'}$ $X_{2'}$ X_5 X_1	10.43i 13.48 18.82 25.22 35.14	X_3 $X_{5'}$ X_5 X_1 $X_{2'}$	39.95 40.32 54.21 64.00 82.44	X_5 $X_{5'}$ $X_{2'}$ X_5 X_1	23.43i 12.89 18.10 24.05 32.24	X_3 $X_{5'}$ X_5 X_1 $X_{2'}$	39.92 40.91 52.20 64.10 77.74
M	$M_{3'}$ $M_{2'}$ $M_{5'}$ M_3 $M_{5'}$ $M_{3'}$	10.54i 13.42 13.73 23.95 35.03 42.15	M_5 M_2 $M_{5'}$ M_1 M_4	44.94 51.99 54.48 56.74 89.09	$M_{3'}$ $M_{2'}$ $M_{5'}$ M_3 $M_{5'}$ $M_{3'}$	20.71i 12.77 12.89 25.79 33.48 41.29	M_5 M_2 $M_{5'}$ M_1 M_4	42.65 43.89 53.93 56.54 84.68
R	R_{15} R_{25} $R_{12'}$	16.48 20.59 47.99	$R_{25'}$ R_{15} $R_{2'}$	49.30 51.45 93.14	R_{15} R_{25} $R_{12'}$	15.87 22.57 38.93	$R_{25'}$ R_{15} $R_{2'}$	47.86 51.33 88.90

Table 18: Longitudinal and transverse interatomic force constants (Ha/Bohr^2) with respect Ti atom (0.5, 0.5, 0.5) along the Ti-O chain of cubic $BaTiO_3$.

Atom	Total Force	DD Force	SR Force
Ti(0)	+0.16887	-0.27936	+0.44823
$O_{\parallel}$(1)	-0.00234	+0.23481	-0.23715
$Ti_{\parallel}$(2)	-0.06979	-0.03732	-0.03246
$O_{\parallel}$(3)	+0.01658	+0.00870	+0.00788
$Ti_{\parallel}$(4)	-0.00854	-0.00467	-0.00388
$O_{\perp}$(1)	-0.01897	-0.04313	+0.02415
$Ti_{\perp}$(2)	+0.00919	+0.01866	-0.00947

4 Concluding Remarks

We report here the structure and equation of state of stable phases of $BaTiO_3$, $PbTiO_3$, $SrTiO_3$, $AgNbO_3$, $Pb_xBa_{8-x}(TiO_3)_8$ and $Sr_xBa_{8-x}(TiO_3)_8$ systems obtained using the PBE flavor of DFT and compared them with available experimental data and previous theoretical calculations. The computations on alloys are also aimed at development of polarizable interaction potentials for molecular dynamics simulations of complex ferroelectric materials and structures (Zhang, 2006 and Majdoub et al., 2008). We find that the Born

Table 19: Computed phonon frequencies (meV) of cubic $AgNbO_3$ at experimental lattice constant of 3.98095 Å at Γ, X, M, R. First frequency column shows the calculated unstable modes.

q-point	Freq.							
Γ	21.65*i* 15.13*i*(*Prosandeev, 2005*)	0.00	5.88	5.91	14.94	42.90	64.26	94.67
X	15.12*i*	3.81 57.81	5.53 101.44	8.31	18.47	27.92	30.12	50.69
M	21.77*i* 12.90*i* 22.81*i*(*Prosandeev, 2005*) 4.22*i*(*Prosandeev, 2005*)	3.57 65.39	4.18 108.53	24.70	29.74	44.23	46.15	54.51
R	21.05*i* 22.07*i*(*Prosandeev, 2005*)	4.84	40.85	44.46	59.58	113.36		

Table 20: Longitudinal and transverse interatomic force constants (Ha/Bohr^2) with respect Nb atom (0.5, 0.5, 0.5) along the Nb-O chain of cubic $AgNbO_3$.

Atom	Total Force	DD Force	SR Force
Nb(0)	+0.20587	-0.49576	+0.70163
$O_{\parallel}(1)$	-0.02868	+0.34970	-0.37838
$Nb_{\parallel}(2)$	-0.10362	-0.05641	-0.04721
$O_{\parallel}(3)$	+0.02370	+0.01295	+0.01012
$Nb_{\parallel}(4)$	-0.01219	-0.00705	-0.00514
$O_{\perp}(1)$	-0.01228	-0.04301	+0.03073
$Nb_{\perp}(2)$	+0.01419	+0.02821	-0.001402

effective charges correlate with the Ti-O bond length and the stability of the ferroelectric phase. We find that the LO-TO mode splitting is related to the dynamical charges and the optical dielectric constant. For, $BaTiO_3$ we report the phonon dispersion relations, leading to soft modes consistent with previous DFT calculations and with available experimental results.

We anticipate that the properties calculated through the use of first principles methods can be used as input for both hierarchical/simultaneous multiscale modeling methods discussed in Ghoniem and Cho (Ghoniem, 2002), Yang and Tewary (Yang, 2006) and Wu and Chen (Wu, 2007).

Acknowledgement: This research was partially supported by grants from ARO-MURI (Engineering Microstructural Complexity in Ferroelectric Devices) and from DARPA-PROM (Predicting Real Optimized Materials).

References

Axe, J. D. (1967): Apparent Ionic Charges and Vibrational Eigenmodes of $BaTiO_3$ and other Per-

ovskites *Phys. Rev., 157*, 429.

Baroni, S., Giannozzi, P., & Testa, A. (1987): Green-Function Approach to Linear Response in solids *Phys. Rev. Lett., 58*, 1861-1864.

Burns, G., & Dacol, F. H. (1982): Polarization in the Cubic Phase of $BaTiO_3$ *Solid State Comm., 42*, 9-12.

Cohen, R. E. (1992): Origin of Ferroelectricity in Perovskite Oxides *Nature, 358*, 136-138.

Cohen, R. E., & Krakauer, H. (1992): Electronic-Structure Studies Of The Differences In Ferroelectric Behavior Of $Batio_3$ And $Pbtio_3$ *Ferroelectrics, 136*, 65-83.

Cooper, P. R., Grinberg, I., & Rappe, A. M. (2003): In P. K. Davies & D. J. Singh (Eds.), *Fundamental Physics of Ferroelectrics* (Vol. CP677):

Fischer, G. J., Wang, Z., & Karato, S.-I. (1993): Elasticity Of Catio3, Srtio3 And Batio3 Perovskites Up To 3.0 Gpa - The Effect Of Crystallographic Structure *Phys. Chem. Minerals, 20*, 97-103.

Frazer, B. C. (1962): Neutron Diffraction Studies Of Ferroelectrics *J. Phys. Soc. Japan, SB-II*, 376.

Fu, H., & Gülseren, O. (2002): Piezoelectric Pb(Zr0.5Ti0.5)O-3: Interplay of atomic ordering, ferroelectric soft modes, and pressure *Phys. Rev. B, 66*, 214114.

Garcia, A., & Vanderbilt, D. (1996): First-principles study of stability and vibrational properties of tetragonal PbTiO3 *Phys. Rev. B, 54*, 3817-3824.

Ghoniem, N.M. & Cho N.M. (2002): The Emerging Role of Multiscale Modeling in Nano- and Micro-mechanics of Materials, *CMES: Computer Modeling in Engineering & Sciences* Vol.3, 147-174.

Ghosez, P., Cockayne, E., Waghmare, U. V., & Rabe, K. M. (1999): Lattice dynamics of BaTiO3, PbTiO3, and PbZrO3: A comparative first-principles study *Phys. Rev. B, 60,* 836-843.

Ghosez, P., & Gonze, X. (2000): Band-by-band decompositions of the Born effective charges *J. Phys.: Condens. Matter, 12*, 9179-9188.

Ghosez, P., Gonze, X., Lambin, P., & Michenaud, J.-P. (1995): Born Effective Charges Of Barium-Titanate - Band-By-Band Decomposition And Sensitivity To Structural Features *Phys. Rev. B, 51*, 6765-6768.

Ghosez, P., Gonze, X., & Michenaud, J.-P. (1998): Ab initio phonon dispersion curves and interatomic force constants of barium titanate *Ferroelectrics, 206*, 205-217.

Ghosez, P., Gonze, X., & Michenaud, J.-P. (1999): First-principles characterization of the four phases of barium titanate *Ferroelectrics, 220*, 1-15.

Ghosez, P., Michenaud, J.-P., & Gonze, X. (1998): Dynamical atomic charges: The case of ABO(3) compounds *Phys. Rev. B, 58*, 6224.

Giannozzi, P., de Gironcoli, S., Pavone, P., & Baroni, S. (1991): Abinitio Calculation Of Phonon Dispersions In Semiconductors *Phys. Rev. B 43*, 7231-7242.

Gonze, X., Allan, D. C., & Teter, M. P. (1992): Dielectric Tensor, Effective Charges, And Phonons In Alpha-Quartz By Variational Density-Functional Perturbation-Theory *Phys. Rev. Lett., 68*, 3603-3606.

Gonze, X., Beuken, J.-M., Caracas, R., Detraux, F., Fuchs, M., Rignanese, G.-M., et al. (2002): First-principles computation of material properties: the ABINIT software project *Computational Materials Science, 25*, 478-492.

Gonze, X., Charlier, J.-C., Allan, D. C., & Teter, M. P. (1994): Interatomic Force-Constants From First Principles - The Case Of Alpha-Quartz *Phys. Rev. B, 50*, 13035-13038.

Gonze, X., Rignanese, G.-M., Verstraete, M., Beuken, J.-M., Pouillon, Y., Caracas, R., et al. (2005): A brief introduction to the ABINIT software package *Zeit. Kristallogr., 220*, 558-562.

Gray, R. W. (1949): U.S. Patent No. 2 486 560.

Grinberg, I., Ramer, N. J., & Rappe, A. M. (2000): Transferable relativistic Dirac-Slater pseudopotentials *Phys. Rev. B, 62*, 2311-2314.

Harada, J., Pedersen, T., & Barnea, Z. (1970): X-Ray And Neutron Diffraction Study Of Tetragonal Barium Titanate *Acta Cryst., A26*, 336.

Harrison, W. A. (1980): *Electronic Structure and the Properties of Solids*. San Fransisco: Freeman.

Hellwege, K. H., & Hellwege, A. M. (Eds.): (1969): *Landolt-Bornstein* (Vol. 3): Berlin: Springer.

Henry, N. F. M., & Lonsdale, K. (Eds.): (1952): *International Tables for X-Ray Crystallography* (Vol. I): Birmingham, England: The Kynoch Press.

Hohenberg, P., & Kohn, W. (1964): Inhomogeneous Electron Gas *Phys. Rev., 136*, 864A.

Hudson, L. T., Kurtz, R. L., Robey, S. W., Temple, D., & Stockbauer, R. L. (1993): Surface Core-Level Shifts Of Barium Observed In Photoemission Of Vacuum-Fractured Batio3(100) *Phys. Rev. B, 47*, 1174.

Jannot, B., Escribe-Filippini, C., & Bouillot, J. (1984): Lattice-Dynamics Of Pure Barium-Titanate And Barium Strontium-Titanate Solid-Solutions *J. Phys. C: Solid State Phys., 17*, 1329-1337.

Kahn, A. H., & Leyendecker, J. (1964): Electronic Energy Bands In Strontium Titanate *Phys. Rev., 135*, A1321.

Kato, H., Kobayashi, H., & Kudo, A. (2002): Role of Ag+ in the band structures and photocatalytic properties of AgMO3 (M: Ta and Nb) with the perovskite structure *J. Phys. Chem. B, 106*, 12441-12447.

Khenata, R., Sahnoun, M., Baltache, H., Rerat, M., Rashek, A. H., Illes, N., et al. (2005): First-principle calculations of structural, electronic and optical properties of BaTiO3 and BaZrO3 under hydrostatic pressure *Solid State Communications, 136*, 120-125.

King-Smith, R. D., & Vanderbilt, D. (1992): A 1st-Principles Pseudopotential Investigation Of Ferroelectricity In Barium-Titanate *Ferroelectrics, 136*, 85-94.

King-Smith, R. D., & Vanderbilt, D. (1993): THEORY OF POLARIZATION OF CRYSTALLINE SOLIDS *Phys. Rev. B, 47*, 1651.

Kohn, W., & Sham, L. J. (1965): Self-Consistent Equations Including Exchange And Correlation Effects *Phys. Rev., 140*, 1133B.

Kresse, G., & Furthmüller, J. (1996): Efficient iterative schemes for ab initio total-energy calculations using a plane-wave basis set *Phys. Rev. B, 54*, 11169-11186.

Kresse, G., & Hafner, J. (1993): Abinitio Molecular-Dynamics For Liquid-Metals *Phys. Rev. B, 47*, RC 558-561.

Kresse, G., & Joubert, J. (1999): From ultrasoft pseudopotentials to the projector augmented-wave method *Phys. Rev. B, 59*, 1758-1775.

Kuroiwa, Y., Aoyagi, S., & Sawada, A. (2001): Evidence for Pb-O covalency in tetragonal PbTiO3 *Phys. Rev. Lett., 87*, 217601.

Kwei, G. H., Lawson, A. C., Billinge, S. J. L., & Cheong, S. W. (1993): Structures Of The Ferroelectric Phases Of Barium-Titanate *J. Phys. Chem., 97*, 2368.

Lasota, C., Wang, C.-Z., Yu, R., & Krakauer, H. (1997): Ab initio linear response study of SrTiO3 *Ferroelectrics, 194*, 109.

Lee, C., Ghosez, P., & Gonze, X. (1994): Lattice-Dynamics And Dielectric-Properties Of Incipient Ferroelectric Tio2 Rutile *Phys. Rev. B, 50*, 13379-13387.

Li, Z., Grimsditch, M., Foster, C. M., & Cha, S. K. (1996): Dielectric and elastic properties of ferroelectric materials at elevated temperature *J. Phys. Chem. Solids, 57*, 1433-1438.

Lyddane, R. H., Sachs, R. G., & Teller, E. (1941): On the polar vibrations of alkali halides *Phys. Rev., 59*, 673-676

Majdoub, MS; Sharma, P.; Cagin, T. (2008): Enhanced size-dependent piezoelectricity and elasticity in nanostructures due to the flexoelectric effect Physical Review B, in press (2008):

Mattheiss, L. F. (1972): Energy-Bands For Knif3, Srtio3, Kmoo3, And Ktao3 *Phys. Rev. B, 6*, 4718-4740.

Meister, J., & Schwarz, W. H. E. (1994): Principal Components Of Ionicity *J. Phys. Chem., 98*, 8245-8252.

Michel-Calendini, F. M., Chermette, H., & Weber, J. (1980): Molecular-Orbital Studies Of Abo3 Perovskites By The Scf-Ms-X-Alpha Method - Local-Densities Of States, Chemical Bonding And Optical-Transitions *J. Phys. C, 13*, 1427-1441.

Migoni, R. L., Bilz, H., & Bauerle, D. (1976): *Phys. Rev. Lett., 37*, 1155.

Mitsumi et al., T. (1981): *Oxides, Landolt-Bornstein Numerical Data and Functional Relationships in Science and Technology, Group III,* (Vol. 16 Pt. a): Berlin: Springer Verlag.

Monkhorst, H. J., & Paack, J. D. (1976): Pecial Points For Brillouin-Zone Integrations *Phys. Rev. B, 13*, 5188-5192.

Nemoshkalenko, V. V., & Timoshevskii, A. N. (1985): The Peculiarities Of The Electronic-Structure Of Batio3 In The Catio3, Srtio3, Batio3 Series *Physica Status Solidi B, 127*, 163-173.

Payne, M. C., Teter, M. P., Allan, D. C., Arias, T. A., & Joannopoulos, J. D. (1992): Iterative Minimization Techniques For Abinitio Total-Energy Calculations - Molecular-Dynamics And Conjugate Gradients *Rev. Mod. Phys., 64*, 1045-1097.

Peng, C. H., Chang, J. F., & Desu, S. (1992): *Proceedings of The Materials Research Society* (Vol. 243): Materials Research Society.

Perdew, J. P., Burke, K., & Ernzerhof, M. (1996): *Phys. Rev. Lett., 77*, 3865.

Pertosa, P., & Michel-Calendini, F. M. (1978): X-Ray Photoelectron-Spectra, Theoretical Band Structures, And Densities Of States For Batio3 And Knbo3 *Phys. Rev. B, 17*, 2011-2020.

Piskunov, S., Heifets, E., Eglitis, R. I., & Borstel, G. (2004): Bulk properties and electronic structure of SrTiO3, BaTiO3, PbTiO3 perovskites: an ab initio HF/DFT study *Comp. Mater. Sci., 29*, 165-178.

Posternak, M., Resta, R., & Baldereschi, A. (1994): Role Of Covalent Bonding In The Polarization Of Perovskite Oxides - The Case Of Knbo3 *Phys. Rev. B, 50*, 8911-8914.

Press, W. H., Flannery, B. P., Teukolsky, S. A., & Vetterling, W. T. (1986): *Numerical Recipes*. New York: Cambridge University Press.

Prosandeev, S. A. (2005): Comparative analysis of the phonon modes in AgNbO3 and NaNbO3 *Physics of the Solid State, 47*, 2130-2134.

Pruzan, P., Gourdain, D., Chrvin, J. C., Canny, B., Couzinet, B., & Hanfland, M. (2002): Equation of state of BaTiO3 and KNbO3 at room temperature up to 30 GPa *Solid State Communications, 123*, 21-26.

Rappe, A. M., Rabe, K. M., Kaxiras, E., & Joannopoulos, J. D. (1990): Optimized Pseudopotentials *Phys. Rev. B, 41*, 1227-1230.

Ratuszna, A., Pawluk, J., & Kania, A. (2003): Temperature evolution of the crystal structure of $AgNbO_3$ *Phase Transitions, 76*, 611-620.

Ricci, D., Bano, G., Pacchioni, G., & Illas, F. (2003): Electronic structure of a neutral oxygen vacancy in SrTiO3 *Phys. Rev. B, 68*, 224105.

Rose, J. H., Smith, J. R., Guinea, F., & Ferrante, J. (1984): Universal Features Of The Equation Of State Of Metals *Phys. Rev. B, 29*, 2963-2969.

Saghi-Szabo, G., Cohen, R. E., & Krakauer, H. (1998): First-principles study of piezoelectricity in tetragonal PbTiO3 *Ferroelectrics, 206*(1):

Sciau, P., Kania, A., Dkhil, B., Suard, E., & Ratuszna, A. (2004): Structural investigation of AgNbO3 phases using x-ray and neutron diffraction *J. Phys.: Condens. Matter, 16*, 2795-2810.

Shirane, G., Danner, H., & Pepinsky, P. (1957): Neutron Diffraction Study Of Orthorhombic Batio3 *Phys. Rev., 105*, 856-860.

Shirane, G., Frazer, B. C., Minkiewicz, V. J., & Leake, J. A. (1967): Soft Optic Modes In Barium Titanate *Phys. Rev. Lett., 19*, 234.

Tinte, S., Stachiotti, M. G., Sepliarsky, M., Migoni, R. L., & Rodriguez, C. O. (1999): Atomistic modelling of BaTiO3 based on first-principles calculations *J. Phys.: Condens. Matter, 11*, 9679.

Uludoğan, M., Cagin, T., & Goddard III, W. A. (2002): Ab initio studies on phase behavior of Barium Titanate, in *Perovskite Materials*, Eds. Alexandra Navrotsky, Kenneth R. Poeppelmeier and Renata M. Wentzcovitch.

Valasek, J. (1921): Piezo-electric and allied phenomena in Rochelle salt. *Phys. Rev., 17*, 475-481.

Vanderbilt, D., & King-Smith, R. D. (1993): Electric Polarization As A Bulk Quantity And Its Relation To Surface-Charge *Phys. Rev. B, 48*, 4442.

Veithen, M., Gonze, X., & Ghosez, P. (2002): Electron localization: Band-by-band decomposition and application to oxides *Phys. Rev. B, 66*, 235113.

Waghmare, U. V., & Rabe, K. M. (1997): Ab initio statistical mechanics of the ferroelectric phase transition in PbTiO3 *Phys. Rev. B, 55*, 6161.

Wemple, S. H. (1970): Polarization Fluctuations And Optical-Absorption Edge In Batio3 *Phys. Rev. B, 2*, 2679.

Weyrich, K. H., & Siems, R. (1985): Deformation Charge-Distribution And Total Energy For Perovskites *Z. Phys. B, 61*, 63-68.

Wu, K.C. & Chen, S.H. (2007): Two Dimensional Dynamic Green's Functions for Piezoelectric Materials, *CMES: Computer Modeling in Engineering & Sciences*, Vol. 20, 147-156.

Yang, B. & Tewary, V.K. (2006): Efficient Green's Function Modeling of Line and Surface Defects in Multilayered Anisotropic Elastic and Piezoelectric Materials, *CMES: Computer Modeling in Engineering & Sciences*, Vol.15, 165-178

Yu, R., & Krakauer, H. (1995): First-Principles Determination Of Chain-Structure Instability In $KNbO_3$ *Phys. Rev. Lett., 74*, 4067-4070.

Zein, N. E. (1984): Density Functional Calculations Of Crystal Elastic Modula And Phonon-Spectra *Sov. Phys., Solid State, 26*, 1825.

Zhang, Q. (2004): *Atomistic Simulations of $BaTiO_3$*. California Institute of Technology, Pasadena, Calfornia.

Zhang, Q., Cagin T., Goddard W.A. (2006): The Ferroelectric Phases in Ferroelectrics are also anti-ferroelectric," *Proceedings of National Academy of Sciences* USA vol **103**, 14695-14700.

Zhong, W., King-Smith, R. D., & Vanderbilt, D. (1994): Giant Lo-To Splitting Sin Perovskite Ferroelectrics *Phys. Rev. Lett., 72*, 3618-3621.